

Goal-Oriented Error Control and Mesh Adaptivity for Stationary Fluid-Structure Interaction Using a deal.II-FROSch Implementation

Sebastian Kinnewig^[0000-0002-0923-7413],
Thibaut Klenke^[0009-0009-8790-8145],
Thomas Wick^[0000-0002-1102-6332]

1 Introduction

Fluid-structure interaction (FSI) is a well-known multidomain problem in which different physics interact. In this contribution, our focus will be on goal-oriented a posteriori error control using the dual-weighted residual (DWR) method [3] using a partition-of-unity (PU) localization [15]. For applications of the DWR method in fluid-structure interaction, we refer to [9, 8, 19, 13, 14, 7, 18, 2].

The main objective in this work is on a parallel efficient linear solver. While often in our prior work on adaptivity and local mesh refinement, sparse direct solvers were utilized, this still limits the treatment of large-scale problems. Specifically, in prior work [18], within Newton's method, the arising linear systems were solved with a sequential sparse direct solver. The major extension is two-fold. First, we employ a parallel Schwarz preconditioner within the GMRES iterative solver, which replaces the sparse direct solver. Therefore, we utilize the restricted additive Schwarz (RAS) preconditioner that is accessible via the deal.II-FROSch interface developed in [10, 12]. Second, we apply that framework to locally refined meshes obtained from the DWR adaptivity. We notice that locally refined meshes have not been tested in our prior work [10]. The basis of our programming code is [16] (see also updates on GitHub <https://github.com/tommeswick/fsi>) and we take some ideas from deal.II [1] step-14. Our resulting code can be found on GitHub <https://github.com/tommeswick/goal-oriented-fsi>.

Sebastian Kinnewig · Thibaut Klenke · Thomas Wick
Leibniz University Hannover, Institute for Applied Mathematics, Welfengarten 1, 30167 Hannover, Germany, e-mail: kinnewig@ifam.uni-hannover.de, thibaut.klenke@stud.uni-hannover.de, thomas.wick@ifam.uni-hannover.de

2 Variational-monolithic ALE fluid-structure interaction

We denote by $\Omega := \Omega(t) \subset \mathbb{R}^d$, $d = 2$, the total domain with $\Omega_f(t)$ and $\Omega_s(t)$. The FSI-interface between $\Omega_f(t)$ and $\Omega_s(t)$ is denoted by $\Gamma_i(t) = \overline{\partial\Omega_f(t)} \cap \overline{\partial\Omega_s(t)}$. Let $I_T := (0, T)$ with the end time value $T > 0$. We define the arbitrary Lagrangian-Eulerian (ALE) time-derivative as the total derivative of an Eulerian field: $\partial_t|_{\widehat{\mathcal{A}}} v_f(x, t) = \widehat{w} \cdot \nabla v_f + \partial_t v_f(x, t)$, where the mesh velocity is defined by $\widehat{w} := \partial_t \widehat{\mathcal{A}}$ with the ALE mapping $\widehat{\mathcal{A}}(\widehat{x}, t) = \widehat{x} + \widehat{u}_f(\widehat{x}, t)$ and $\widehat{u}_f : \widehat{\Omega}_f \rightarrow \mathbb{R}^d$. The ‘hat’ variables are defined in the ALE reference domains $\widehat{\Omega}$, $\widehat{\Omega}_f$ and $\widehat{\Omega}_s$. Then, the isothermal, incompressible Navier-Stokes equations in an ALE setting read: Find $v_f : \Omega_f(t) \times I_T \rightarrow \mathbb{R}^d$ and $p_f : \Omega_f(t) \times I_T \rightarrow \mathbb{R}$ such that

$$\begin{aligned} \rho_f \partial_t|_{\widehat{\mathcal{A}}} v_f + \rho_f (v_f - \widehat{w}) \cdot \nabla v_f - \nabla \cdot \sigma_f(v_f, p_f) &= 0, & \nabla \cdot v_f &= 0 & \text{in } \Omega_f(t) \times I_T, \\ v_f^D &= v_{in} \text{ on } \Gamma_{in}, \quad v_f = 0 \text{ on } \Gamma_D, \quad -p_f n_f + \rho_f \nu_f \nabla v_f \cdot n_f = 0 \text{ on } \Gamma_{out}, \quad v_f = v_s \text{ on } \Gamma_i, \\ v_f(0) &= v_0 \text{ in } \Omega_f(0), \end{aligned}$$

where the (symmetric) Cauchy stress is given by

$$\sigma_f(v_f, p_f) := -pI + \rho_f \nu_f (\nabla v + \nabla v^T),$$

with the density ρ_f and the kinematic viscosity ν_f , and the normal vector n_f . Moreover, I denotes the identity matrix in two dimensions. The equations for geometrically nonlinear elastodynamics are given as follows: Find $\widehat{u}_s : \widehat{\Omega}_s \times I_T \rightarrow \mathbb{R}^d$ such that

$$\begin{aligned} \widehat{\rho}_s \partial_t^2 \widehat{u}_s - \widehat{\nabla} \cdot (\widehat{F} \widehat{\Sigma}) &= 0 & \text{in } \widehat{\Omega}_s \times I_T, \\ \widehat{u}_s &= 0 \text{ on } \widehat{\Gamma}_D, \quad \widehat{F} \widehat{\Sigma} \cdot \widehat{n}_s = \widehat{J} \sigma_f \widehat{F}^{-T} \cdot \widehat{n}_s \text{ on } \widehat{\Gamma}_i, \quad \widehat{u}_s(0) = \widehat{u}_0, \quad \widehat{v}_s(0) = \widehat{v}_0 \text{ in } \widehat{\Omega}_s \times \{0\}, \end{aligned}$$

with the second Piola-Kirchhoff stress tensor

$$\widehat{\Sigma} = \widehat{\Sigma}_s(\widehat{u}_s) = 2\mu \widehat{E} + \lambda \text{tr}(\widehat{E})I, \quad \widehat{E} = \frac{1}{2}(\widehat{F}^T \widehat{F} - I), \quad \widehat{F} = I + \widehat{\nabla} \widehat{u}_s, \quad \widehat{J} := \det(\widehat{F}).$$

Here, μ and λ are the Lamé coefficients for the solid. The solid density is denoted by $\widehat{\rho}_s$. Furthermore, \widehat{n}_s denotes the normal vector.

3 Discretization and numerical solution

3.1 Discretization

For the spatial discretization, a conforming Galerkin finite element method (FEM) on quadrilateral mesh elements is employed. Specifically, we use Q_2^c elements for

\widehat{v} and $\widehat{u} := \widehat{u}_f + \widehat{u}_s$, and Q_1^c elements for \widehat{p} . For the flow problem $(\widehat{v}, \widehat{p})$, this is the well-known inf-sup stable Taylor-Hood element. Due to variational-monolithic coupling ([14, 17]) and globally-defined finite elements, the fluid pressure must be extended to the solid domain, which is achieved via $\alpha_u[(\widehat{\nabla}\widehat{p}_s, \widehat{\nabla}\widehat{\psi}^p) + (\widehat{p}_s, \widehat{\psi}^p)]$, where α_u (as before) is a small positive parameter. An alternative to the (artificial) pressure extension is to work with the FE_NOTHING element in deal.II.

3.2 Solution via Newton-GMRES with Schwarz preconditioning

This subsection is the main novelty in comparison to our prior work [18] on goal-oriented error control and adaptivity in stationary fluid-structure interaction. The nonlinear problem is solved with Newton's method. For algorithmic descriptions of the implementation, we refer to [16]. Inside Newton's method, in the defect step, we must solve linear equation systems. In this work, we utilize GMRES (generalized minimal residuals) with Schwarz preconditioning. In more detail, we decompose the computational domain $\widehat{\Omega}$ into N non-overlapping subdomains $\widehat{\Omega}_1, \dots, \widehat{\Omega}_N$. In our case, this decomposition was obtained using the graph partitioning tool `p4est` [4]. Alternatively, this decomposition could be obtained via a geometrical approach. Next, the subdomains are extended by k layers of elements providing an overlapping domain decomposition with subdomains $\widehat{\Omega}'_1, \dots, \widehat{\Omega}'_N$. The overlap size is denoted by $\delta = kh$, where h represents the mesh parameter. Moreover, we define the local finite element spaces \widehat{V}_i on the local overlapping subdomains. By this construction, it follows that $\widehat{V}_i \subset \widehat{V}$, so the restriction operators $R_i : \widehat{V} \rightarrow \widehat{V}_i$ and corresponding prolongation operators $P_i : \widehat{V}_i \rightarrow \widehat{V}$ can be defined for all $1 \leq i \leq N$. Note that $P_i = R_i^T$ is the transposed operator of R_i and both can be represented as sparse binary matrices. Next, we define \widehat{P}_i such that $\sum_{i=1}^N \widehat{P}_i R_i = I$. Using this notation, the restricted additive Schwarz (RAS) preconditioner introduced by Cai and Sarkis [5] is formally written as

$$M_{\text{RAS}}^{-1} = \sum_{i=1}^N \widehat{P}_i A_i^{-1} R_i, \quad (1)$$

where in the case of local exact solvers, $A_i := R_i A P_i \quad \forall 1 \leq i \leq N$ is the local subdomain matrix, and A is the global system matrix, resulting from the FEM discretization of the FSI problem from Section 2.

4 PU-DWR goal-oriented error control

Based on the FSI problem from Section 2, let $\widehat{A}(\cdot)(\cdot)$ and $\widehat{F}(\cdot)$ denote the PDE and the right hand side in weak form, respectively [18, 16]. The Galerkin approximation reads: Find $\widehat{U}_h = \{\widehat{v}_{f,h}, \widehat{u}_{f,h}, \widehat{u}_{s,h}, \widehat{p}_{f,h}\} \in \widehat{X}_{h,D}^0$, where $\widehat{X}_{h,D}^0 := \{\widehat{v}_{f,h}^D + \widehat{V}_{f,\widehat{v},h}^0\} \times \{\widehat{u}_{f,h}^D + \widehat{V}_{f,\widehat{u},h}^0\} \times \{\widehat{u}_{s,h}^D + \widehat{V}_{s,h}^0\} \times \widehat{L}_{f,h}^0$, such that

$$\hat{A}(\hat{U}_h)(\hat{\Psi}_h) = \hat{F}(\hat{\Psi}_h) \quad \forall \hat{\Psi}_h \in \hat{X}_h, \quad (2)$$

where \hat{X}_h is the test space with homogeneous Dirichlet conditions.

4.1 Goal functional

The solution \hat{U}_h is used to calculate an approximation $J(\hat{U}_h)$ of the goal-functional $J(\hat{U}) : \hat{X} \rightarrow \mathbb{R}$. This functional is assumed to be sufficiently differentiable. The drag value as goal functional reads

$$J(\hat{U}) := \int_{\hat{S}} \hat{J} \hat{\sigma}_f \hat{F}^{-T} \hat{n}_f \hat{d} \, d\hat{s},$$

where \hat{n}_f is the outward point normal vector of the cylinder boundary \hat{S} [11] and the FSI interface $\hat{\Gamma}_i$. Moreover, \hat{d} is a unit vector perpendicular to the mean flow direction. For the drag, we use $\hat{d} = (1, 0)$.

4.2 Error representation

We use the (formal) Euler-Lagrange method to derive a computable representation of the approximation error $J(\hat{U}) - J(\hat{U}_h)$. The task is: Find $\hat{U} \in \hat{X}_D^0$ such that

$$\min\{J(\hat{U}) - J(\hat{U}_h)\} \quad \text{s.t.} \quad \hat{A}(\hat{U})(\hat{\Psi}) = \hat{F}(\hat{\Psi}) \quad \forall \hat{\Psi} \in \hat{X},$$

from which we obtain the optimality system

$$\mathcal{L}'_{\hat{Z}}(\hat{U}, \hat{Z})(\delta\hat{Z}) = \hat{F}(\delta\hat{Z}) - \hat{A}(\hat{U})(\delta\hat{Z}) = 0 \quad \forall \delta\hat{Z} \in \hat{X}, \quad (\text{Primal problem}),$$

$$\mathcal{L}'_{\hat{U}}(\hat{U}, \hat{Z})(\delta\hat{U}) = J'(\hat{U})(\delta\hat{U}) - \hat{A}'_{\hat{U}}(\hat{U})(\delta\hat{U}, \hat{Z}) = 0 \quad \forall \delta\hat{U} \in \hat{X}, \quad (\text{Adjoint problem}).$$

Proposition 1 ([3]). *We have the error identity:*

$$J(\hat{U}) - J(\hat{U}_h) = \frac{1}{2} \rho(\hat{U}_h)(\hat{Z} - \hat{\Phi}_h) + \frac{1}{2} \rho^*(\hat{U}_h, \hat{Z}_h)(\hat{U} - \hat{\Psi}_h) + \mathcal{R}_h^{(3)}, \quad (3)$$

for all $\{\hat{\Psi}_h, \hat{\Phi}_h\} \in \hat{X}_h \times \hat{X}_h$ and with the primal and adjoint residuals:

$$\begin{aligned} \rho(\hat{U}_h)(\hat{Z} - \hat{\Phi}_h) &:= -A(\hat{U}_h)(\cdot) + \hat{F}(\cdot), \\ \rho^*(\hat{U}_h, \hat{Z}_h)(\hat{U} - \hat{\Psi}_h) &:= J'(\hat{U}_h)(\cdot) - A'(\hat{U}_h)(\cdot, \hat{Z}_h) + \hat{F}(\cdot). \end{aligned}$$

The remainder term $\mathcal{R}_h^{(3)}$ is of cubic order. This error identity can be used to define the error estimator η , which can be further utilized to design adaptive schemes.

Moreover, the primal error identity, that we utilize in this work, reads:

$$J(\widehat{U}) - J(\widehat{U}_h) = \eta = \rho(\widehat{U}_h)(\widehat{Z} - \widehat{\Phi}_h) + \mathcal{R}_h^{(2)}, \quad (4)$$

where the remainder term $\mathcal{R}_h^{(2)}$ is of quadratic order [3].

4.3 Adjoint equation, discretization, and numerical solution

The adjoint equation reads: Find $\widehat{Z} = (\widehat{z}^v, \widehat{z}^u, \widehat{z}^p) \in \widehat{X}$ such that

$$J'(\widehat{U})(\widehat{\Phi}) = \widehat{A}'_{\widehat{G}}(\widehat{U})(\widehat{\Phi}, \widehat{Z}) \quad \forall \widehat{\Phi} \in \widehat{X}.$$

For the discretization, we briefly mention that higher-order information for the adjoint solution must be employed due to Galerkin orthogonality; in this work $\widehat{X}_h \subset \widehat{X}_h^{\text{high}} \subset \widehat{X}$. For simplicity, this is realized with global higher-order finite elements and in order to ensure again inf-sup stability, we use Q_4^c elements for \widehat{z}^v and \widehat{z}^u , and Q_2^c elements for \widehat{z}^p . It is clear that this is an expensive choice. For the numerical solution, the same solvers as for the primal problem are taken (see Section 3.2), namely a Newton-type method and GMRES with RAS preconditioning. Since the adjoint problem is linear, Newton's method converges in one step.

4.4 Localization

A PU localization [15] for stationary FSI reads:

Proposition 2. *We have for the primal error part $\rho(\widehat{U}_h)(\cdot)$ the a posteriori error estimate*

$$|J(\widehat{U}) - J(\widehat{U}_h)| \leq |\eta_h^{\text{high}}| := \left| \sum_{i=1}^M \eta_i \right| \leq \sum_{i=1}^M |\eta_i| := |\eta_{\text{ind}}| \quad (5)$$

where η_h^{high} is the so-called practical error estimator; for the notation "practical" error estimator, we refer to [6]. Moreover, M is the dimension of the PU finite element space \widehat{V}_{PU} (composed of Q_1^c functions χ_i) and with the PU-DoF indicators

$$\begin{aligned} \eta_i &= -A(\widehat{U}_h)((\widehat{Z}_h^{\text{high}} - i_h \widehat{Z}_h^{\text{high}})\widehat{\Psi}_i) + \widehat{F}((\widehat{Z}_h^{\text{high}} - i_h \widehat{Z}_h^{\text{high}})\widehat{\Psi}_i) \\ &= -(\widehat{\rho}_f \widehat{J}(\widehat{F}^{-1} \widehat{v}_f \cdot \widehat{\nabla}) \widehat{v}_f), \widehat{\psi}_i^v)_{\widehat{\Omega}_f} - (\widehat{J} \widehat{\sigma}_f \widehat{F}^{-T}, \widehat{\nabla} \widehat{\psi}_i^v)_{\widehat{\Omega}_f} + (\widehat{g}_f, \widehat{\psi}_i^v)_{\widehat{\Gamma}_N} \\ &\quad - (\widehat{F} \widehat{\Sigma}, \widehat{\nabla} \widehat{\psi}_i^v)_{\widehat{\Omega}_s} - (\widehat{\sigma}_{\text{mesh}}, \widehat{\nabla} \widehat{\psi}_i^u)_{\widehat{\Omega}_f} - (\widehat{\text{div}}(\widehat{J} \widehat{F}^{-1} \widehat{v}_f), \widehat{\psi}_i^p)_{\widehat{\Omega}_f} \\ &\quad + (\widehat{\rho}_f \widehat{J} \widehat{f}_f, \widehat{\psi}_i^v)_{\widehat{\Omega}_f} + (\widehat{\rho}_s \widehat{f}_s, \widehat{\psi}_i^v)_{\widehat{\Omega}_s} \end{aligned}$$

with the interpolation $i_h : \widehat{X}_h^{\text{high}} \rightarrow \widehat{X}_h$ and the weighting functions are defined as

$$\widehat{\psi}_i^v := (\phi_{2h,v}^{\text{high}} - \phi_{h,v})\chi_i, \quad \widehat{\psi}_i^u := (\phi_{2h,u}^{\text{high}} - \phi_{h,u})\chi_i, \quad \widehat{\psi}_i^p := (\phi_{2h,p}^{\text{high}} - \phi_{h,p})\chi_i.$$

4.5 Adaptive algorithm

1. Compute the primal solution \widehat{U}_h on the present mesh \mathcal{T}_h .
2. Compute the (higher-order) adjoint solution $\widehat{Z}_h^{(2)}$ on the present mesh \mathcal{T}_h .
3. Evaluate $\eta_h^{\text{high}} := \sum_i \eta_i$ in (5).
4. Check if the stopping criterion is satisfied: $|J(\widehat{U}) - J(\widehat{U}_h)| \leq |\eta_h^{\text{high}}| \leq \text{TOL}$, then accept \widehat{U}_h within the tolerance TOL. Otherwise, proceed to the following step.
5. Mark all elements K_i for refinement that touch DoFs i with indicator η_i with $\eta_i \geq \frac{\alpha \eta_h^{\text{high}}}{M_{\text{el}}}$ (where M_{el} denotes the total number of elements of the mesh \mathcal{T}_h and $\alpha \approx 1$).

5 Numerical test: FSI-1 benchmark

In this section, we consider the FSI-1 benchmark [11]. The drag value is taken as the goal functional $J(\widehat{U})$. The configuration, all parameters, and reference values can be found in [11]. The reference value for computing the true error was computed on an eight-times adaptively refined mesh and is $J_{\text{ref}}(\widehat{U}) = 15.3612$. The graphical solution of the primal problem, including the adaptively refined mesh, is displayed in Figure 1.

As an example, for the solution of the primal problem on 8 subdomains and an overlap of around 20%, we have on the finest level with 373 081 DoFs, and the solution of the nonlinear problem required 13 Newton iterations and took around 9.2 min, where on average 34 GMRES iterations were required. Our results for the adjoint problem are displayed in Table 1. During our computations, we observed efficiency dependencies on the hardware setup, which is not unusual in parallel computations, e.g., communication cost, but require careful future investigations, specifically due to the locally refined meshes and the structure of the adjoint problem.

Our results for the error estimation are displayed in Table 2. Therein, we observe well both the error and estimator reductions. The effectivity and indicator indices are not uniformly bounded as it is often observed for nonlinear problems. The main reason is that we work with the primal error part only, rather with the primal and adjoint parts.

As we employed a one-level RAS preconditioner without coarse-grid correction, the method does not scale well, especially the adjoint problem remains challenging. However as overall conclusion, the deal.II-FROSch framework is promising for locally refined meshes obtained from a posteriori error control.

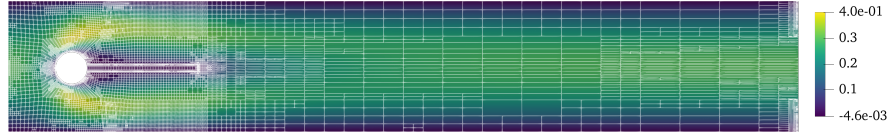


Fig. 1 FSI-1 benchmark: The adaptive mesh is displayed together with the primal solution of \widehat{v}_x .

Adjoint DoFs	$t_{\text{direct}}^{\text{walltime}}$	$t_{20\%}^{\text{walltime}}$	$n_{20\%}^{\text{GMRES}}$	$t_{40\%}^{\text{walltime}}$	$n_{40\%}^{\text{GMRES}}$
52 052	5.11 s	7.50 s	30	14.23 s	14
81 272	6.39 s	14.68 s	55	26.02 s	16
142 423	22.68 s	30.26 s	27	50.27 s	16
249 979	45.66 s	57.80 s	30	66.35 s	16
425 322	124.80 s	152.87 s	58	217.85 s	17
681 434	243.00 s	293.78 s	56	448.02 s	17
993 769	443.40 s	515.05 s	57	762.66 s	18
1 413 226	1141.20 s	934.69 s	120	990.09 s	29

Table 1 Comparison of walltimes and number of iterations of a direct solver (KLU2) and a FROSch-preconditioned iterative solver for the adjoint problem. The overlap refers to the approximate overlap at the last refinement step.

Primal DoFs	$J_{\text{ref}}(\widehat{U}) - J(\widehat{U}_h)$	η_h^{high}	η_{ind}	I_{eff}	I_{ind}
13 310	2.49e-01	1.43e-01	4.37e-01	5.74e-01	1.75e+00
20 921	8.10e-02	4.73e-02	1.58e-01	5.84e-01	1.95e+00
37 108	2.31e-02	1.14e-02	5.84e-02	4.94e-01	2.53e+00
65 374	9.51e-03	4.92e-03	2.70e-02	5.18e-01	2.84e+00
111 513	4.43e-03	2.50e-03	1.51e-02	5.65e-01	3.40e+00
179 273	2.11e-03	1.35e-03	9.13e-03	6.39e-01	4.33e+00
261 856	9.91e-04	7.76e-04	5.89e-03	7.83e-01	5.95e+00
373 081	3.49e-04	5.07e-04	3.80e-03	1.45e+00	1.09e+01

Table 2 Results for the error estimation. The effectivity index I_{eff} and indicator index I_{ind} are defined for example in [15], respectively.

References

1. Africa, P.C., Arndt, D., Bangerth, W., Blais, B., Fehling, M., Gassmüller, R., Heister, T., Heltai, L., Kinnewig, S., Kronbichler, M., et al.: The deal.ii library, version 9.6. *J. Numer. Math.* **32**(4) (2024)
2. Ahuja, K., Endtmayer, B., Steinbach, M., Wick, T.: Multigoal-oriented error estimation and mesh adaptivity for fluid–structure interaction. *J. Comput. Appl. Math.* **412**, 114315 (2022)
3. Becker, R., Rannacher, R.: An optimal control approach to a posteriori error estimation in finite element methods. *Acta Numer.* pp. 1–102 (2001)
4. Burstedde, C., Wilcox, L.C., Ghattas, O.: p4est: scalable algorithms for parallel adaptive mesh refinement on forests of octrees. *SIAM J. Sci. Comput.* **33**(3), 1103–1133 (2011)
5. Cai, X.C., Sarkis, M.: A restricted additive Schwarz preconditioner for general sparse linear systems. *SIAM J. Sci. Comput.* **21**(2), 792–797 (1999)

6. Endtmayer, B., Langer, U., Wick, T.: Two-side a posteriori error estimates for the dual-weighted residual method. *SIAM J. Sci. Comput.* **42**(1), A371–A394 (2020)
7. Failer, L., Wick, T.: Adaptive time-step control for nonlinear fluid–structure interaction. *J. Comput. Phys.* **366**, 448–477 (2018)
8. Fick, P., van Brummelen, E., Zee, K.: On the adjoint-consistent formulation of interface conditions in goal-oriented error estimation and adaptivity for fluid–structure interaction. *Comput. Methods Appl. Mech. Eng.* **199**, 3369–3385 (2010)
9. Grätsch, T., Bathe, K.J.: Goal-oriented error estimation in the analysis of fluid flows with structural interactions. *Comput. Methods Appl. Mech. Eng.* **195**, 5673–5684 (2006)
10. Heinlein, A., Kinnewig, S., Wick, T.: Coupling deal.ii and frosch: a sustainable and accessible (O)ras preconditioner. *ACM Trans. Math. Softw.* **51** (4), 22 (2025)
11. Hron, J., Turek, S.: Proposal for numerical benchmarking of fluid–structure interaction between an elastic object and laminar incompressible flow. In: *Fluid–Structure Interaction*, pp. 146–170. Springer (2006)
12. Kinnewig, S.: Domain decomposition solvers for electromagnetic and multi-physics problems. Ph.D. thesis, Leibniz University Hannover (2025)
13. Richter, T.: Goal-oriented error estimation for fluid–structure interaction problems. *Comput. Methods Appl. Mech. Eng.* **223–224**, 28–42 (2012)
14. Richter, T.: *Fluid-Structure Interactions: Models, Analysis, and Finite Elements*. Springer (2017)
15. Richter, T., Wick, T.: Variational localizations of the dual-weighted residual estimator. *J. Comput. Appl. Math.* **279**, 192–208 (2015)
16. Wick, T.: Solving monolithic fluid–structure interaction problems in arbitrary ALE coordinates with the deal.II library. *Arch. Numer. Softw.* **1**, 1–19 (2013)
17. Wick, T.: *Multiphysics Phase-Field Fracture: Modeling, Adaptive Discretizations, and Solvers*. De Gruyter, Berlin, Boston (2020)
18. Wick, T.: Adjoint-based methods for optimization and goal-oriented error control applied to fluid–structure interaction: implementation of a partition-of-unity dual-weighted residual estimator for stationary forward fsI problems in deal.ii. In: *Book of Extended Abstracts of the 6th ECCOMAS Young Investigators Conference*. ECCOMAS, Valencia, Spain (2021)
19. van der Zee, K., van Brummelen, E., Akkerman, I., de Borst, R.: Goal-oriented error estimation and adaptivity for fluid–structure interaction using exact linearized adjoints. *Comput. Methods Appl. Mech. Eng.* **200**(37), 2738–2757 (2011)